

# Coded excitation ultrasonic needle tracking: an *in vivo* study

Wenfeng Xia<sup>1,a</sup>, Yuval Ginsberg<sup>2</sup>, Simeon J. West<sup>3</sup>, Daniil I. Nikitichev<sup>1</sup>,

Sebastien Ourselin<sup>4</sup>, Anna L. David<sup>2</sup>, and Adrien E. Desjardins<sup>1</sup>

<sup>1</sup>*Department of Medical Physics and Biomedical Engineering,*

*University College London, Gower Street,*

*London WC1E 6BT, United Kingdom.*

<sup>2</sup>*Institute for Women's Health, University College London,*

*86-96 Chenies Mews, London WC1E 6HX, United Kingdom.*

<sup>3</sup>*Department of Anaesthesia, University College Hospital,*

*Main Theatres, Maple Bridge Link Corridor, Podium 3,*

*235 Euston Rd, London NW1 2BU, United Kingdom. and*

<sup>4</sup>*Center for Medical Imaging Computing,*

*University College London, Gower Street,*

*London WC1E 6BT, United Kingdom.*

---

<sup>a</sup> Author for correspondence: wenfeng.xia@ucl.ac.uk

## Abstract

**Purpose:** Accurate and efficient guidance of medical devices to procedural targets lies at the heart of interventional procedures. Ultrasound imaging is commonly used for device guidance, but determining the location of the device tip can be challenging. Various methods have been proposed to track medical devices during ultrasound-guided procedures, but widespread clinical adoption has remained elusive. With ultrasonic tracking, the location of a medical device is determined by ultrasonic communication between the ultrasound imaging probe and a transducer integrated into the medical device. The signal-to-noise ratio (SNR) of the transducer data is an important determinant of the depth in tissue at which tracking can be performed. In this paper, we present a new generation of ultrasonic tracking in which coded excitation is used to improve the SNR without spatial averaging.

**Methods:** A fiber optic hydrophone was integrated into the cannula of a 20 gauge insertion needle. This transducer received transmissions from the ultrasound imaging probe, and the data was processed to obtain a tracking image of the needle tip. Excitation using Barker or Golay codes was performed to improve the SNR, and conventional bipolar excitation was performed for comparison. The performance of the coded excitation ultrasonic tracking system was evaluated in an *in vivo* ovine model with insertions to the brachial plexus and the uterine cavity.

**Results:** Coded excitation significantly increased the SNRs of the tracking images, as compared with bipolar excitation. During an insertion to the brachial plexus, the SNR was increased by factors of 3.5 for Barker coding and 7.1 for Golay coding. During insertions into the uterine cavity, these factors ranged from 2.9 to 4.2 for Barker coding and 5.4 to 8.5 for Golay coding. The maximum SNR was 670, which was obtained with Golay coding during needle withdrawal from the brachial plexus. Range sidelobe artifacts were observed in tracking images obtained with Barker coded excitation, and they were visually absent with Golay coded excitation. The spatial tracking accuracy was unaffected by coded excitation.

**Conclusion:** Coded excitation is a viable method for improving the SNR in ultrasonic tracking without compromising spatial accuracy. This method provided SNR increases that are consistent with theoretical expectations, even in the presence of physiological motion. With the ultrasonic tracking system in this study, the SNR increases will have direct clinical implications in a broad range of interventional procedures by improving visibility of medical devices at large depths.

45 Key words: image guided interventions, ultrasound imaging, medical device tracking, coded  
excitation, fiber optic hydrophone

## I. INTRODUCTION

Ultrasound (US) imaging is commonly used to guide needle insertions in a wide range  
of clinical contexts. However, needle tips can readily stray from the US imaging plane,  
50 particularly when they are at large depths and when the needles are thin [1]. Lack of  
ultrasonic visibility of the needle tip can result in significant complications, and it can  
reduce procedural efficiency.

Procedures in which needle visualization is of particular importance include nerve blocks  
for regional anesthesia and interventional pain management [1–3], and minimally invasive  
55 interventions within the uterus for amniotic fluid sampling, chorionic villus sampling, and  
fetal surgery [4, 5]. With nerve blocks, loss of visibility of the needle tip can result in mechan-  
ical trauma to nerve fascicles [6], local anesthetic toxicity following inadvertent intravascular  
injections [7], and pneumothorax [8]. Ultrasound-guided uterine access can be particularly  
challenging in cases with oligohydramnios, when the practitioner is inexperienced, and when  
60 the mother is obese. Needle tip visualization could also be helpful with percutaneous um-  
bilical blood sampling (cordocentesis) and multifetal pregnancy reduction, where needle tip  
movements with high precision are required.

Improving the visibility of medical devices under US guidance has attracted increasing  
research interest in the past decade [9–31]. Echogenic needles, which have surface modifica-  
65 tions to improve US scattering, can provide visibility improvements when the needle tip is  
in-plane. However, this method still results in incomplete visualization: in a recent study on  
nerve blocks in patients, echogenic needle tips were visible in less than 56% of the procedure  
time [9]. Automatic needle recognition can be performed in two- and three-dimensional  
US images [10]; it can be facilitated with mechanical constraints [11–13] and with camera  
70 pose estimation [14], but challenges can arise when the needle has a similar appearance to  
surrounding tissues.

Several active methods for needle tracking have been investigated. Electromagnetic (EM)  
tracking allows for pre-puncture planning, but this method can be highly inaccurate in the  
presence of EM field disturbances from commonplace metal objects such as tables or surgical

75 instruments [15]. Additional methods include inducing motion of the needle [16–20] and generating ultrasound waves from the needle with photoacoustic excitation [21–23]. Active methods confer the potential advantage of providing tracking information that is not present in conventional US images.

Ultrasonic tracking (UT) is an active method for determining the position of a medical  
80 device with the potential to overcome many limitations of current methods. It involves reception or transmission of US pulses by the medical device in concert with transmission or reception by an US imaging probe. In one configuration, transmissions were triggered by an integrated US sensor [24]. Triangulation or beamforming algorithms can be used to obtain positional information in the coordinate system of the US imaging probe [25–27]. We  
85 previously demonstrated that UT can be performed with a fiber optic hydrophone (FOH) integrated into the needle tip [28–31]. This FOH can readily be miniaturized ( $<125\ \mu\text{m}$  outer diameter) for integration into small diameter needles.

As visualization of needles often becomes more challenging when the tips are deeper in tissue, it is important to optimize the signal-to-noise (SNR) of UT systems. Coded excitation  
90 can be used to improve the SNR of B-mode US images, with potential increases of 15-20 dB [32–34]. This technique allows for temporal averaging to be performed within one or two transmissions, in a more efficient manner than averaging across multiple transmissions with bipolar excitation [35].

In this paper, Barker and Golay codes were used to increase the SNR in UT. These codes  
95 were applied to transmissions by individual transducer elements of an imaging probe, and reception was performed with a fiber optic hydrophone integrated into a needle. The SNR improvements were compared to theoretical expectations, and to values obtained with non-coded, bipolar pulses. The performance of the system was tested in an *in vivo* ovine model with needle insertions to the brachial plexus and to several intrauterine targets.

## 100 II. MATERIALS AND METHODS

### A. Ultrasonic tracking system

The UT system was centered on a clinical US imaging system (SonixMDP, Analogic Ultrasound, Richmond, BC, Canada) with a 6.5 MHz linear array imaging probe (L9-4/38, 9-

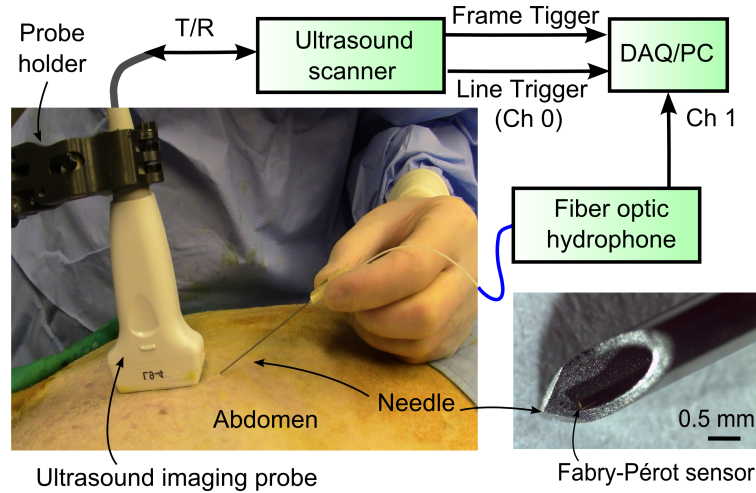


FIG. 1. Schematic of the ultrasonic tracking system showing the practitioner performing the needle insertion through the abdomen of a sheep *in vivo*.

4 MHz bandwidth, 300  $\mu\text{m}$  pitch, Analogic Ultrasound, Richmond, BC, Canada). The FOH, which had an outer diameter of 125  $\mu\text{m}$  at its distal end, (Precision Acoustics, Dorchester, UK), comprised a Fabry-Pérot cavity at the distal end that was interrogated by a tunable, continuous wave laser [36]. It was fixated within the cannula of a 20 gauge injection needle (Terumo, Surrey, UK) so that its distal end was flush with the bevel surface (Figure 1), and fixated with a small quantity of epoxy applied proximal to the Fabry-Pérot cavity. The cannula remained patent after application of the epoxy; fluid aspiration and delivery with the cannula were possible but they were not performed in this study. With the FOH protected by the surrounding cannula, its performance was found to be unchanged after repeated insertions.

Ultrasonic transmissions for tracking were controlled by a custom program written in Labview (National Instruments, Austin, Texas), which accessed low-level libraries to specify excitation sequences that were provided to individual transducer elements sequentially. B-mode US imaging was implemented with a commercial imaging software on the US system. The FOH signals were digitized at 100 MS/s by a DAQ card (USB-5132; National Instruments, Austin, Texas). A detailed description of the tracking system can be found in Ref. [31].

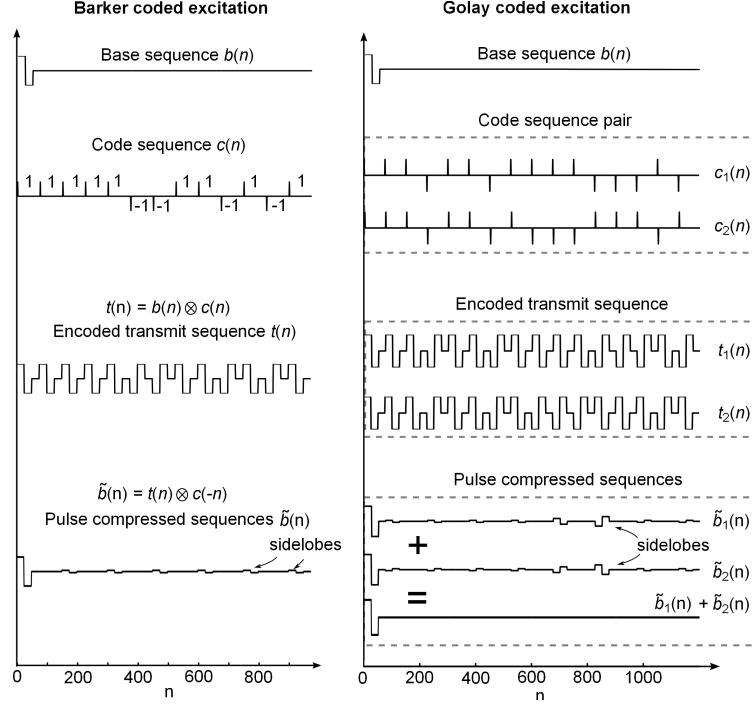


FIG. 2. Illustration of the processes of Barker and Golay coded excitation.

## B. Coded excitation

In this study, coded excitation of US transmissions were performed with digital pulse compression schemes. Coded sequences of pulses were transmitted from each transducer element of the imaging probe, the transmissions were received by the FOH, and subsequently pulse compression was performed on the FOH signals. Two different types of sequences were used: Barker codes and Golay code pairs.

With Barker coding, the 13-bit coded excitation sequence  $c(n)$  was convolved with a bipolar base sequence  $b(n) = [1, -1, 0]$  to obtain the encoded transmission sequence  $t(n)$ :

$$t(n) = b(n) \otimes c(n) \quad (1)$$

where  $n \in \mathbf{N}$ . This encoded transmission sequence was provided as input to the US transmission elements. The transmitted pressure waveform from the transducer element can be modeled as a convolution of the  $t(n)$  with the temporal response of a transducer element to impulse excitation,  $h(n)$ . The corresponding FOH signal (Figure 3b and d),  $f(n)$ , was assumed to be proportional to that transmitted pressure waveform:

$$f(n) \propto t(n) \otimes h(n) \quad (2)$$

To obtain Eq. 2, the frequency response of the FOH signal was assumed to be flat over the range of transmitted frequencies.

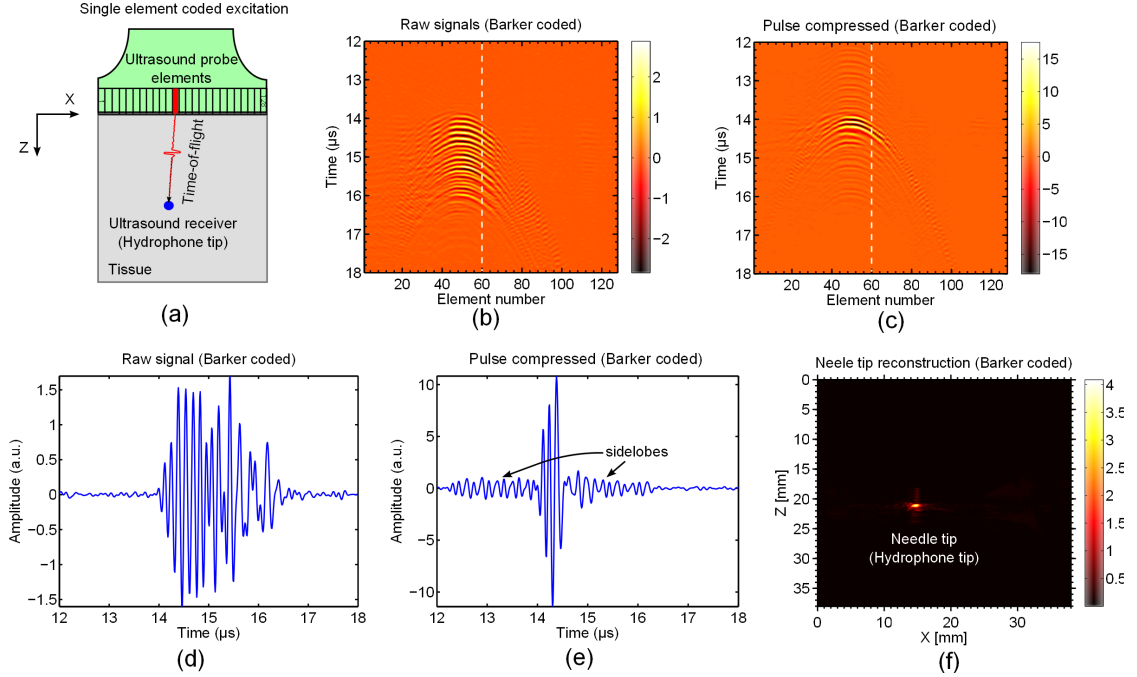


FIG. 3. Schematic illustration of the coded excitation algorithms (with Barker coding as an exam-  
 140 ple) including: (a) transmission from single transducer elements of the ultrasound imaging probe  
 with coded excitation; (b) detection of 128-channel raw signals using the fiber optic hydrophone; (c)  
 pulse compression of the raw signals; (d) a representative channel signal [dashed line in (b) and (c)]  
 before pulse compression; (e) the signal in (d) after pulse compression; (f) k-Wave reconstruction  
 of the tracking image using the pulse compressed signals.

145 To perform pulse compression,  $f(n)$  was convolved with the time-reversed version of the  
 oversampled coded sequence  $c(-n)$ . Thus, the pulse compressed base sequence  $\tilde{b}(n)$  can be  
 expressed as:

$$\tilde{b}(n) = t(n) \otimes c(-n) \quad (3)$$

as shown in Figure 2. Notably,  $\tilde{b}(n)$  has a mainlobe which has the same shape as the base  
 150 sequence  $b(n)$ , with the amplitude increased by a factor of 13 (Figure 2a). The FOH signals

after pulse compression (Figure 3c and e) were thus proportional to the convolution of the pulse compressed sequence  $\tilde{b}(n)$  with  $h(n)$ :

$$\tilde{f}(n) \propto \tilde{b}(n) \otimes h(n) \quad (4)$$

Golay coded excitation was similar, except that it involved a pair of codes, with two  
 155 corresponding US transmissions. Pulse compression was performed to each FOH signal and paired results were added. The length of each Golay sequence was limited to 32 bits due to limitations imposed by the low-level software libraries (Figure 2b).

The expected SNR increase conferred by coded excitation is determined by the total code length,  $N$ . Coded excitation involves addition of both signal and noise terms. The signal  
 160 terms add coherently so that they increase in direct proportion to  $N$ . Provided that the noise terms are uncorrelated, the standard deviation of the total variance increases with  $\sqrt{N}$ . As such, the expected SNR increase is proportional to  $N/\sqrt{N} = \sqrt{N}$ . In the case of Golay coded excitation, the total code length is the sum of the lengths of the code pairs. Therefore, for Barker and Golay coded excitation, the expected SNR increases are  $\sqrt{13} = 3.6$   
 165 and  $\sqrt{32 \times 2} = 8$ , respectively.

Transmissions for coded, non-coded, and B-mode US (bi-polar excitation) were performed sequentially. Barker coding was performed first (128 transmissions, one for each transducer element); Golay coding, second ( $2 \times 128$ , which included a pair for each transducer element); bi-polar excitation, third (128). Following the transmissions for tracking, a standard  
 170 transmission sequence was performed for B-mode US imaging (128).

Processing of the digitized FOH data was performed with a custom program written in MATLAB (Natick, NH, USA). The pulse compressed signals were processed with the k-Wave toolbox [37] to obtain an image of the needle tip (Figure 3f). A commercial beam-forming algorithm was used for B-mode US imaging. The needle tip positions were marked as red  
 175 crosses according to the positions of the maxima of the tracking images, and overlaid on the corresponding B-mode US images in real-time.

### C. Experiments

To evaluate the performance of the system in clinically relevant conditions, UT was performed during needle insertions to the brachial plexus and into the uterine cavity of

180 a pregnant sheep *in vivo*. All procedures on animals were conducted in accordance with U.K. Home Office regulations and the Guidance for the Operation of Animals (Scientific Procedures) Act (1986). Ethics approval was provided by the joint animal studies committee of the Royal Veterinary College and the University College London, United Kingdom. These experiments were performed in the context of a separate study, for which the animal was  
185 obtained. Two pregnant ewes of Romney breed were studied. Ewes were time-mated after receiving intravaginal progesterone suppositories for 2 weeks to induce ovulation. At 100 and 114 days of gestation, (term, 145 days of gestation) they underwent general anesthesia induced with 1 g of thiopentone administered intravenously and after intubation; the ewes were then maintained on halothane 2% in oxygen, and finally underwent terminal anesthesia.

190 All procedures were performed under US imaging. After clipping the fleece and cleaning, fetal biometry was assessed where appropriate and used to confirm the correct gestational age according to standard measurements as described [38]. Subsequently, the needle containing the hydrophone was inserted. An insertion to the brachial plexus was performed at an angle of 40 degrees, followed by withdrawal along the same trajectory. Intra-uterine insertions  
195 were performed at angles in the range of 27 to 66 degrees. A total of 6 intrauterine targets were reached with separate insertions, including amniotic fluid and 5 targets in the fetus: the muscle (femur), the right ventricle of the heart [38], the trachea [39], the umbilical vein [40], and the stomach [41]. Across all insertions, the needle tip depth ranged from 10 to 41 mm. Correct needle placement was confirmed by aspiration of the appropriate cavity fluid  
200 (amniotic, stomach or tracheal fluid; blood) or by injection of 1 mL of normal saline, during which time microbubbles were observed within the tissues.

For each insertion, the SNRs of the tracking images were estimated. A  $2\text{ mm} \times 2\text{ mm}$  area enclosing the hydrophone tip was defined as the signal region, and a  $2\text{ mm} \times 2\text{ mm}$  region outside the signal region was defined as the noise region; the SNR was calculated  
205 as the ratio of the maximum amplitude of the image values in the signal region and the standard deviation of the image values in the noise region.

As the US and UT images are inherently co-registered, the tracking accuracy was estimated as the spatial resolution with which the needle tip could be visualized. To estimate the spatial resolution, the axial and lateral profiles of reconstructed needle tracking images  
210 were obtained and the corresponding full-width at half-maximum (FWHM) values were calculated.

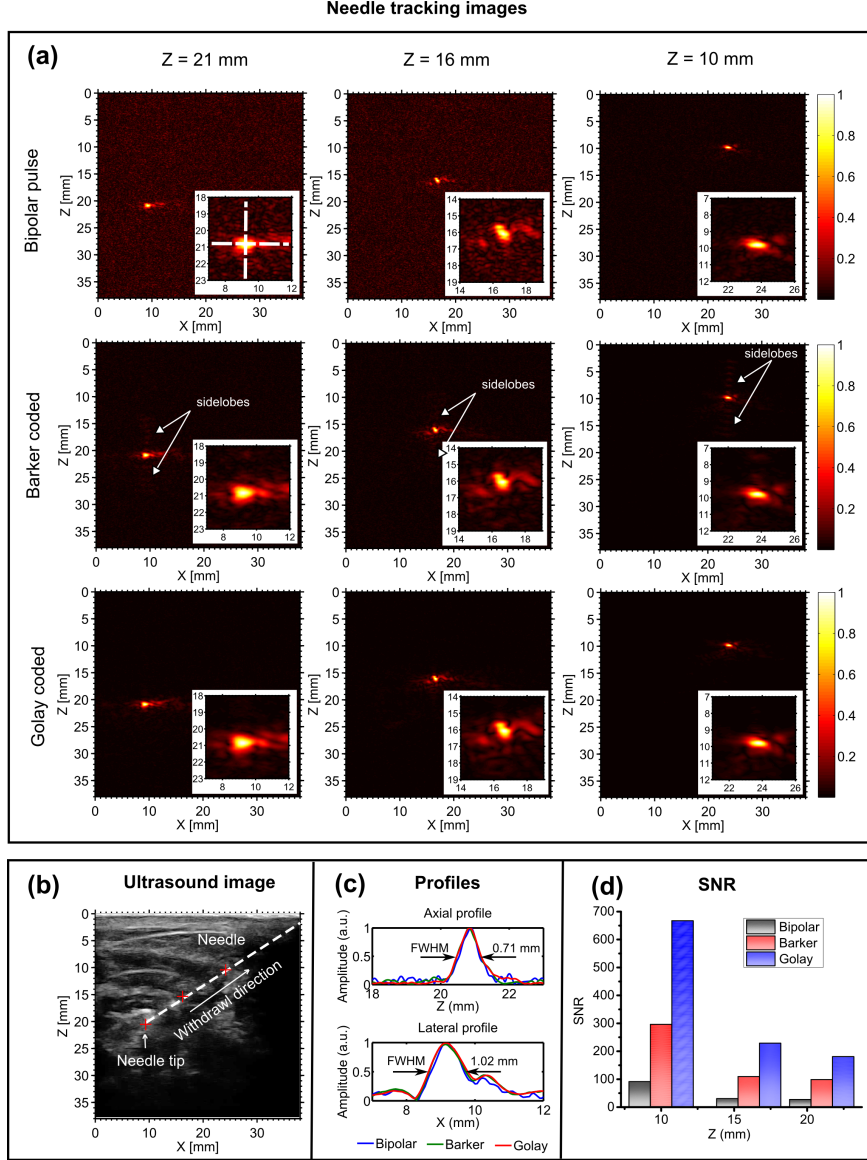


FIG. 4. (a) Tracking images obtained during an insertion in the context of brachial plexus nerve blocks in a sheep in vivo. Tracking images were obtained at three different depths during needle withdrawal (right to left), for three different excitation codes: single cycle bipolar wave, Barker coding, and Golay coding (top to bottom). The dimensions of the insets at the bottom-right of all tracking images have dimensions of  $4 \text{ mm} \times 4 \text{ mm}$ . (b) Needle tip positions are marked as red crosses according to the positions of the maxima of the tracking images. Image artifacts induced by the range sidelobes in Barker coded images are indicated by white arrows. The corresponding B-mode ultrasound image with the needle trajectory is shown in b). The lateral and axial profiles for tracking images obtained at a depth of 21 mm with different excitation methods are compared as in (c). The signal-to-noise ratios (SNRs) for tracking images with different excitation methods and at different depths are compared in (d).

### III. RESULTS

With the needle insertion toward the brachial plexus, the tip was barely visible in the B-mode US images, but it was clearly visible in all tracking images. In the tracking images, the needle tip presented as an elliptical region with high signal amplitudes (Figure 4a). The needle tip positions revealed by the tracking images closely matched the trajectory of the needle insertion visualized in the US images (Figure 4b). The tracking images acquired with the needle tip at a depth of 21 mm show nearly identical axial and lateral profiles for different excitation codes (Figure 4c), with FWHM values of  $0.71 \pm 0.06$  mm and  $1.02 \pm 0.06$  mm (mean  $\pm$  standard deviation), respectively. The SNRs of the tracking images decreased with the insertion depth (Figure 4d), from 91 at a depth of 10 mm, to 27 at a depth of 21 mm, when each element of the transducer array was excited using a bipolar wave. With coded excitation, the SNRs were dramatically increased compared to bipolar wave excitation: for Barker coded excitation, the SNR was increased 3.2-fold to 302 at a depth of 10 mm and 3.5-fold to 98 at a depth of 21 mm; for Golay coded excitation, the SNR was increased 7.1-fold to 670 at a depth of 10 mm and 7.2-fold to 180 at a depth of 21 mm. Image artifacts were observed in the tracking image obtained using Barker coded excitation (Figure 4a, white boxes in the second row), which were consistent with the presence of the range sidelobes using pulse compression. These image artifacts were not observed for tracking images obtained using Golay coded excitation (Figure 4a, the third row).

With needle insertions performed into the uterine cavity, US images could be used to position the needle tip to different target locations (outlines in Figure 5a-f), but the visibility of the needle tip was often poor (Figure 5a-f, left). As with insertions to and from the brachial plexus, the needle tip was presented as an elliptical region with high signal amplitude (Figure 5a-f, inserts and Figure 5h). While axial FWHM values of the tracking images were nearly constant across all insertions ( $0.56 \pm 0.08$  mm), the lateral FWHM values were somewhat larger and more variable ( $1.15 \pm 0.36$ ), with the largest lateral FWHM value of 1.8 mm obtained for the insertion in the muscle femur (Figure 5h). With bipolar wave excitation, the SNRs ranged from 11.5 to 52.1 (Figure 5g). With coded excitation, the SNRs were increased by factors in the ranges of 2.9-4.2 with Barker coded excitation and 5.4-8.5 with Golay coded excitation. The highest SNR was 376.1, which was achieved with Golay coded excitation during an insertion to the umbilical vein.

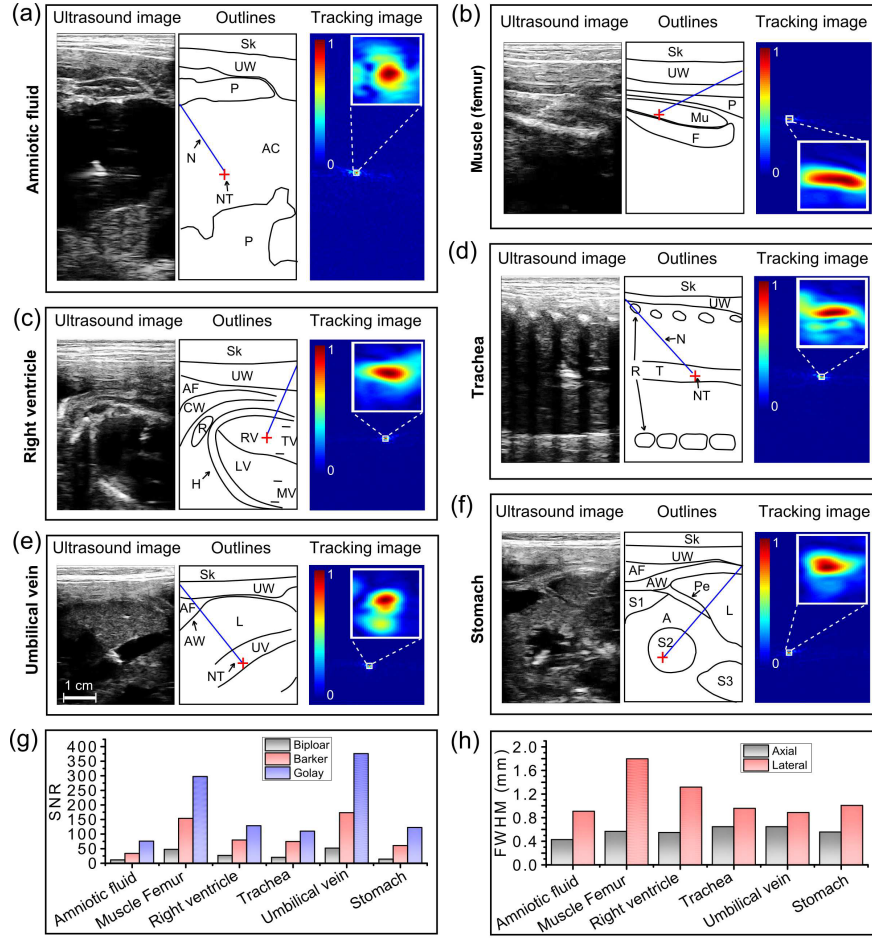


FIG. 5. Ultrasound and tracking images obtained during insertions in the context of fetal interventions in a sheep *in vivo*, including: (a) amniotic fluid at 41 mm; (b) muscle (femur) at 25 mm; (c) right ventricle at 31 mm; (d) trachea at 32 mm; (e) umbilical vein at 33 mm; and (f) stomach at 39 mm. For each insertion, the ultrasound image and the corresponding outlines are on the left; the Golay coded tracking image, on the right. The signal-to-noise ratios (SNRs) and the full width at half maximum (FWHM) values of the lateral and axial profiles for tracking images with different excitation methods (single cycle bipolar wave, Barker coding and Golay coding) are compared in (g) and (h) respectively. The dimensions of inserts in all tracking images are  $2 \text{ mm} \times 2 \text{ mm}$ . Needle tip positions are marked as red crosses according to the positions of maxima in the tracking images. N: Needle; NT: Needle tip; Sk: Skin; UW: Uterine wall; P: Placentome; AC: Amniotic cavity; Mu: Muscle; F: Femur; AF: Amniotic fluid; CW: Chest wall; RV: Right ventricle; LV: Left ventricle; R: Ribs; H: Heart; TV: Tricuspid valve; MV: Mitral valve; T: Trachea; AW: Abdominal wall; L: Liver; UV: Umbilical vein; M: Membrane; A: Abdomen; S1, S2, S3: Stomach; Pe: Peritoneum.

#### IV. DISCUSSION AND CONCLUSIONS

This study demonstrated that coded excitation is an effective method for increasing the  
245 SNR in ultrasonic tracking without incurring an appreciable loss in spatial resolution. This  
study was, to the authors' knowledge, the first in which coded excitation was applied to  
ultrasonic tracking. It was also the first in which ultrasonic tracking was used in the context  
of peripheral nerve blocks and fetal interventions *in vivo*.

The optimal choices for coding and pulse compression schemes depend on the clinical  
250 context. Of the two coding schemes considered in this study, Barker and Golay, the former  
has the advantage of being more efficient, in the sense that it requires only one transmission.  
However, the length of Barker codes is limited to 13, which limits the SNR improvements  
that they can confer. As such, they are best suited to contexts in which acquisition speed is  
of paramount importance. Conversely, Golay codes require pairs of transmissions, but they  
255 are not limited in length. As such, they are best suited for optimising penetration depth.  
Pulse compression schemes could extend beyond the one in this study, to compensate for  
distortions of ultrasonic pulses during propagation through tissue. For instance, mismatched  
filters could be used to compensate for low-pass filtering at large penetration depths [34].

Several differences in the results of coded excitation in B-mode US imaging and UT can be  
260 expected. First, the role of sidelobes that can be introduced by coded excitation may be less  
prominent in UT than in B-mode US imaging, since there is typically only one object within  
a tracking image (which corresponds to the location of the US transducer in the medical  
device). Second, in this study, pulse compression in UT was performed prior to beamform-  
ing, whereas in B-mode US imaging it is typically performed with post-beamformed data.  
265 Beamforming can lead to sub-optimal pulse compression performance [42]. Third, wave  
propagation distortions in UT, such as those resulting from frequency-dependent attenua-  
tion, are likely smaller than those in B-mode US imaging, as propagation occurs in only one  
direction from the imaging probe to the medical device.

With coded excitation, there is a trade-off between the magnitude of the SNR improve-  
270 ment and the sensitivity to motion of the medical device tip relative to the ultrasound  
imaging probe. During ultrasonic tracking, this motion can arise from insertion of the  
device and from physiological motion of tissue surrounding the device. The latter was par-  
ticularly prominent in this study when the needle tip was inside the beating right ventricle

of the ovine fetus. Even under those extreme conditions, the SNR and the resolution of the  
275 tracking images were very similar to those acquired in the presence of much smaller tissue  
motion. This suggests that if hardware had allowed for it, the Golay code length could have  
been increased beyond that in this study whilst retaining insensitivity to tissue motion. As  
suggested in the context of B-mode imaging [43], a hybrid approach could be useful, with  
bipolar or short-length codes used for shallow depths where SNR is high, and longer-length  
280 codes used elsewhere.

The spatial resolution of the needle tracking images in this study was suitable for clinical  
practice. The axial and lateral components of the spatial resolution were smaller than the  
bevel surface length of a 20-gauge injection needle that is commonly used for nerve blocks  
and fetal interventions. The spatial resolution achieved with bipolar excitation in this study  
285 (axial: 0.43 - 0.65 mm; lateral: 0.89 - 1.80 mm) corresponded well to the values obtained in  
a previous study using the same 9-4 MHz linear ultrasound imaging probe (axial 0.40 - 0.58  
mm; lateral: 0.92 - 1.69 mm) [31]. Due to the high sensitivity of the FOH, transmissions  
from the imaging probe were received even when the needle tip was slightly outside the  
2D geometric imaging plane. Therefore, to identify when the needle tip enters this plane,  
290 comparing FOH signals from multiple spatial locations during an insertion could prove  
useful. With additional linear arrays of transducer elements, such as those in 1.5D imaging  
probes, the out-of-plane position of the needle tip could be obtained.

The implementation of ultrasonic tracking in this study has many advantages that make  
it compelling for guiding a wide range of percutaneous procedures, including peripheral  
295 nerve blocks and fetal interventions. The fiber optic hydrophone can be manufactured with  
scalable processes, at low cost; its small diameter and its flexibility make it straightforward  
to integrate into a wide range of medical devices. With a nearly omnidirectional response  
and large bandwidth, it is compatible with a broad range of ultrasound imaging probes  
and medical device angulations. With an absence of electronic components, it is immune  
300 from EM interference. Ultrasonic tracking with coded excitation could be performed with  
other ultrasound sensors, however, including piezoelectric or CMUT transducers. The use  
of coded excitation for ultrasonic tracking will improve needle visualization at large depths,  
where visualization of the medical devices is often most challenging.

## V. ACKNOWLEDGMENTS

305 This work was supported by an Innovative Engineering for Health award by the Wellcome Trust [WT101957] and the Engineering and Physical Sciences Research Council (EPSRC) [NS/A000027/1], by a Starting Grant from the European Research Council [ERC-2012-StG, Proposal 310970 MOPHIM], and by an EPSRC First Grant [EP/J010952/1]. A.L.D. is supported by the UCL/UCLH NIHR Comprehensive Biomedical Research Centre.

310 The authors have no relevant conflicts of interest to disclose.

- 
- [1] K. Chin, A. Perlas, V. Chan, and R. Brull, "Needle visualization in ultrasound-guided regional anesthesia: challenges and solutions," *Reg. Anesth. Pain. Med.* **33**(6), 532–544, (2008).
  - [2] A. G. Randolph, D. J. Cook, C. Gonzales, A. Calle, C. G. Pribble, "Ultrasound guidance for placement of central venous catheters: a meta-analysis of the literature," *Critical Care Medicine* **24**(12), 2053–2058, (1996).
  - 315 [3] S. N. Narouze (Editor), "Atlas of ultrasound-guided procedures in interventional pain management," *Springer, New York*, (2010).
  - [4] S. P. Emery, J. Kreutzer, F. R. Sherman, K. L. Fujimoto, B. Jaramaz, C. Nikou, K. Tobita, B. B. Keller, "Computer-assisted navigation applied to fetal cardiac intervention," *Int. J. Med. Robotics Comput. Assist. Surg.* **3**, 187–198, (2007).
  - 320 [5] Y. Paltieli, S. Degani, A. Zrayek, R. Gonen, M. R. Lewinski, Y. Zamberg, and, G. Ohel, "A new guidance system for freehand, obstetric ultrasound-guided procedures," *Ultrasound Obstet. Gynecol.* **319**, 269–273, (2002).
  - [6] R. Brull, C. J. L. McCartney, V. W. S. Chan, H. El-Beheiry, "Neurological complications after regional anesthesia: contemporary estimates of risk," *Anesth. Analg.* **104**, 965-974, (2007).
  - 325 [7] P. J. Zetlaoui, J. Labbe, and D. Benhamou, "Ultrasound guidance for axillary plexus block does not prevent intravascular injection," *Anesthesiology* **108**(4), 761, (2008).
  - [8] A. Bhatia, J. Lai, V. W. Chan, and R. Brull, "Pneumothorax as a complication of the ultrasound-guided supraclavicular approach for brachial plexus block," *Anesth. Analg.* **111**(3), 817-819, (2010).
  - 330 [9] S. Hebard, and G. Hocking, "Echogenic technology can improve needle visibility during

- ultrasound-guided regional anesthesia,” *Reg. Anesth. Pain. Med.* **36**(2), 185–189, (2011)
- [10] Y. Zhao, C. Cachard, and H. Liebgott, “Automatic needle detection and tracking in 3D ultrasound using an ROI-based RANSAC and Kalman method,” *Ultrasonic Imaging* **35**(4) 283–306, (2013)
- 335 [11] C. Kim, D. Chang, D. Petrisor, G. Chirikjian, M. Han, D. Stoianovici, “Ultrasound probe and needle-guide calibration for robotic ultrasound scanning and needle targeting,” *IEEE Trans. Biomed. Eng.* **60**(6) 1728–1734, (2013)
- [12] V. Stuber, E. M. Suero, T. Hufner, M. Wiewiorski, C. Krettek, M. Citak, “Linear bearing device as a solution for optical navigation of fine needle procedures,” *Technol. Health Care* **18**(4-5) 267–73, (2010).
- 340 [13] M. Abayazid, G. J. Vrooijink, S. Patil, R. Alterovitz, and S. Misra, “Experimental evaluation of ultrasound-guided 3D needle steering in biological tissue,” *Int. J. Comput. Assist. Radiol. Surg.* **9**(6) 931–939, (2014)
- [14] M. Najafi, P. Abolmaesumi, R. Rohling, “Single-camera closed-form real-time needle tracking for ultrasound-guided needle insertion,” *Ultrason. Med. Biol.* **41**(10), 2663–2676, (2015)
- 345 [15] F. Poulin, L. P. Amiot, “Interference during the use of an electromagnetic tracking system under OR conditions,” *J. Biomech.* **35** 733–737, (2002)
- [16] S. M. Klein, M. P. Fronheiser, J. Reach, K. C. Nielsen, S. W. Smith, “Piezoelectric vibrating needle and catheter for enhancing ultrasound-guided peripheral nerve blocks,” *Anesth. Analg.* **105**, 1858–60, (2007).
- 350 [17] V. Rotemberg, M. Palmeri, S. Rosenzweig, S. Grant, D. Macleod, and K. Nightingale, “Acoustic radiation force impulse (ARFI) imaging-based needle visualization,” *Ultrason. Imag.* **33**(1), 1–16 (2011).
- [18] M. P. Fronheiser, S. F. Idriss, P. D. Wolf, and S. W. Smith, “Vibrating interventional device detection using real-time 3-D color Doppler,” *IEEE Trans. Ultrason. Ferroelectr. Freq. Control* **55**(6), 1355–1362, (2008).
- 355 [19] Z. Shen, Y. Zhou, J. Miao, and K. F. Vu, “Enhanced visualization of fine needles under sonographic guidance using a MEMS actuator,” *Sensors* **15** 3107–3115, (2015)
- [20] P. Beigi, R. Rohling, T. Salcudean, V. A. Lessoway, G. C. Ng, “Needle trajectory and tip localization in real-time 3D ultrasound using a moving stylus,” *Ultrason. Med. Biol.* **41**(7), 2057–2070, (2015)
- 360

- [21] J. Su, A. Karpouk, B. Wang and S. Emelianov, “Photoacoustic imaging of clinical metal needles in tissue,” *J. Biomed. Opt.* **15**(2) 021309, (2010)
- 365 [22] W. Xia, D. I. Nikitichev, J. M. Mari, S. J. West, R. Pratt, A. L. David, S. Ourselin, P. C. Beard, and A. E. Desjardins, “Performance characteristics of an interventional multispectral photoacoustic imaging system for guiding minimally invasive procedures,” *J. Biomed. Opt.* **20**(8) 086005, (2015)
- [23] W. Xia, D. I. Nikitichev, J. M. Mari, S. J. West, S. Ourselin, P. C. Beard, and A. E. Desjardins,  
370 “An interventional multispectral photoacoustic imaging platform for the guidance of minimally invasive procedures,” *Proc. SPIE* **9539** 95390D, (2015)
- [24] X. Guo, B. Tavakoli, H. Kang, J. U. Kang, R. E. Cummings and E. M. Boctor “Photoacoustic active ultrasound element for catheter tracking,” *Proc. of SPIE* **8943** 89435M-1, (2014)
- [25] F. Winsberg, H. A. Hitty, R. S. Shapiro, H. C. Yeh, “Use of an of Biopsy Acoustic Needles  
375 Transponder for US Visualization,” *Radiology* **180**3 877–878, (1991)
- [26] S. I. Nikolov, and J. A. Jensen, “Precision of needle tip localization using a receiver in the needle,” *IEEE Int. Ultrason. Sym. Proc.* 479–482, (2008) DOI:10.1109/ULTSYM.2008.0117
- [27] J. Mung, F. Vignon, and A. Jain, “A non-disruptive technology for robust 3D tool tracking for ultrasound-guided interventions,” *Medical Image Computing and Computer-Assisted  
380 Intervention MICCAI* 153-160, (2011)
- [28] W. Xia, C. A Mosse, R. J Colchester, J. M. Mari, D. I. Nikitichev, S. J. West, S. Ourselin, P. C. Beard, A. E Desjardins, “Fiber optic photoacoustic probe with ultrasonic tracking for guiding minimally invasive procedures,” *Proc. SPIE* **9539** 95390K, (2015)
- [29] W. Xia, E. Maneas, D. I. Nikitichev, C. Mosse, G. Sato dos Santos, T. Vercauteren, A.  
385 L. David, S. Ourselin, P. C. Beard, and A. E. Desjardins, “An interventional multispectral photoacoustic imaging platform for the guidance of minimally invasive procedures,” *Medical Image Computing and Computer-Assisted Intervention–MICCAI 2015, Munich, Germany* in press, (2015)
- [30] J. M. Mari, S. West, P. C. Beard, and A. E. Desjardins, “Needle-tip localization using an  
390 optical fibre hydrophone,” *Proc. SPIE* **8983** 893804, (2014)
- [31] W. Xia, J. M. Mari, S. J. West, S. Ourslin, A. E. Desjardins, “In-plane ultrasonic needle tracking using a fiber-optic hydrophone,” *Med. Phys.* **42**(10), 5983-5991, (2015)
- [32] M. O’Donnell “Coded excitation system for improving the penetration of real-time phased-

- array imaging systems,” *IEEE Trans. Ultrason., Ferroelect., Freq. Contr.* **39**, 341351, (1992).
- 395 [33] H. Zhao, L. Y. L. Mo, and S. Gao, “Barker-coded ultrasound color flow imaging: Theoretical and practical design considerations,” *IEEE Trans. Ultrason. Ferroelectr. Freq. Control* **54**(2), 319-331, (2007).
- [34] T. Misarisids, and J. A. Jensen, “Use of modulated excitation signals in medical ultrasound. part I: basic concepts and expected benefits,” *IEEE Trans. Ultrason. Ferroelectr. Freq. Control* **52**(2), 177–191, (2005).
- 400 [35] S. Z. Budisin, “New complementary pairs of sequences,” *Electron. Lett.* **26**(13), 881–883, (1990).
- [36] P. Morris, A. Hurrell, A. Shaw, E. Zhang, P. C. Beard, “A Fabry-Pérot fiber-optic ultrasonic hydrophone for the simultaneous measurement of temperature and acoustic pressure,” *J. Acoust. Soc. Am.* **125**(6) 3611-3622, (2009).
- 405 [37] B. E. Treeby, and B. T. Cox, “k-Wave: MATLAB toolbox for the simulation and reconstruction of photoacoustic wave fields,” *J. Biomed. Opt.* **15**(2), 021314 (2010).
- [38] A. L. David, D. Peebles, M. Miah, M. Themis, M. Nivsarkar, N. Tucker, T. Dahse, T. Cook, C. Coutelle, and C. H. Rodeck, “Ultrasound-guided delivery of viral vectors encoding the beta-galactosidase and human factor IX genes to early gestation fetal sheep in utero. Human Gene Therapy,” *Human Gene Therapy* **364**, 353–364, (2002).
- 410 [39] A. L. David, B. Weisz, L. Gregory, M. Themis, T. Cook, X. Roubliova, J. Deprest, C. Coutelle, C. H. Rodeck, and D. M. Peebles, “Ultrasound-guided injection and occlusion of the trachea in fetal sheep,” *Ultrasound Obstet. Gynecol.* **28**(1), 82–88, (2006).
- 415 [40] A. L. David, J. McIntosh, D. M. Peebles, T. Cook, S. Waddington, B. Weisz, V. Wigley, K. Abi-Nader, M. Boyd, A. M. Davidoff, and A. C. Nathwani, “Recombinant adeno-associated virus-mediated in utero gene transfer gives therapeutic transgene expression in the sheep,” *Human Gene Therapy* **22**, 419–426, (2011).
- [41] A. L. David, D. M. Peebles, L. Gregory, S.N. Waddington, M. Themis, B. Weisz, A. Ruthe, L. Lawrence, T. Cook, C.H. Rodeck, and C. Coutelle, “Clinically applicable procedure for gene delivery to fetal gut by ultrasound-guided gastric injection: toward prenatal prevention of early-onset intestinal diseases,” *Human Gene Therapy* **17**(7), 767–779, (2006).
- 420 [42] T. Azuma, Y. Miwa, and S. Umemura, “Subaperture decoding to enhance performance of coded excitation,” *IEEE Ultrasonics Symposium* **2**, 1669-1672, (2002).

- 425 [43] R. Y. Chiao, and X. Hao, “Coded excitation for diagnostic ultrasound: a system developer’s perspective,” *IEEE Ultrasonics Symposium* **1**, 437-448, (2003). DOI:10.1109/ULTSYM.2003.1293440
- [44] N. A. H. K. Rao, “Investigation of a pulse compression technique for medical ultrasound: A simulation study,” *Med. Phys. Eng. Comp.* **32**(2), 181–188, (1994).